Effect of pressure in the autothermal catalytic partial oxidation of CH_4 and C_3H_8: Spatially resolved temperature and composition profiles

A. Donazzi [a], D. Livio [a], C. Diehm [a,b], A. Beretta [a,*], G. Groppi [a], P. Forzatti [a]

[a] *Department of Energy, Politecnico di Milano, Piazza Leonardo da Vinci 32, 20133 Milan, Italy*
[b] *Institute for Chemical Technology and Polymer Chemistry, Karlsruhe Institute of Technology, Kaiserstrasse 12, Karlsruhe, Germany*

Received 2 August 2013
Received in revised form
23 September 2013
Accepted 27 September 2013
Available online 6 October 2013

1. Introduction

The catalytic partial oxidation of hydrocarbons (CPO) into H_2 or syngas (H_2/CO mixtures) holds great promise in view of a more efficient exploitation of energy resources, especially in the field of small-scale applications. Operation under pressure would strongly benefit the intensification of the process, the minimization of the reactor volume and its integration into more complex systems [1,2]. The use of LPG (propane and butane) and logistic fuels (gasoline, kerosene and diesel) would be of further advantage, as a consequence of their easy storage and distribution as liquids. The main drawbacks that currently hinder the extensive use of light hydrocarbons are the high temperature levels reached on the catalyst surface, which cause deactivation by sintering, and the formation of coke-precursors [3,4]. These species can lead to growth of carbon deposits and are mainly formed by gas phase cracking reactions. Pressure increase is then a major challenge, since it increases the temperature of the catalyst, owing to thermodynamics, and promotes the kinetics of the gas phase chemistry, owing to the fact that the rates scale as a squared function of the pressure ($\propto P^2$) [5,6].

In the literature, few works regarding the CPO of CH_4 are dedicated to the effect of pressure [7–11]. The majority of these works discuss exclusively integral data, that is, data collected at the outlet of the catalytic monolith (typically, a foam or a honeycomb supported catalyst, Rh- or Pt-based). The results agree on the negative effect of pressure on the conversion of CH_4, which decreases when the pressure of the system increases. In line with the expected thermodynamic behavior, this decrease is accompanied by the increase of the outlet temperature and by a drop of the selectivity to syngas, more or less pronounced depending on the experimental conditions (e.g. heat losses of the reactor, geometrical characteristics of the support). At higher O_2/C ratio, the hindering effect of pressure is retained, even though it is weaker. These results are associated to the negative effect of pressure on the steam reforming activity of the catalyst, which results in lower heat removal and lower syngas production. Emphasis is also given to the effect of pressure on the transport properties and on the kinetics of the reaction. In this respect, it is worthy to note that the experiments are generally

* Corresponding author. Tel.: +39 2 23993284; fax: +39 2 23993318.
E-mail addresses: alessandra.beretta@polimi.it (A. Beretta), gianpiero.groppi@polimi.it (G. Groppi).

performed at fixed mass flow rate, meaning that the volumetric flow rate of the gas decreases at increasing pressure and that the residence time becomes longer. In an early work dedicated to CH_4 CPO experiments performed between 1 and 6 bar over 80 ppi Rh-coated foams, Dietz and Schmidt [8] noted that pressure has a very limited effect on the mass transfer rate: considering that diffusive limitations play a significant role in the reaction, the authors argued that longer residence times of the reactants at high temperatures could in principle favor the activation of gas phase chemistry. Fichtner et al. [9] investigated the CPO of CH_4 over a microstructured honeycomb catalyst made of Rh foils. The application of a microreactor and of a specially designed micromixer allowed the authors to explore the reaction up to 20 bar, with both CH_4/air and CH_4/O_2 mixtures. Likely due to the very peculiar testing conditions (channel dimensions of ~100 μm, 0.2–3 ms residence times and high conductivity of the honeycomb), the authors found that mass transport limitations were not significant and suggested that pressure has an inhibiting effect on the kinetics of CH_4 consumption, possibly associated to the formation of carbon deposits on the catalyst surface.

More informative results were accomplished by application of spatially resolved techniques. By means of an in-situ axially resolved Raman/LIF technique, Mantzaras and coworkers [12,13] investigated the CPO of CH_4 over Rh-based catalysts, between 4 and 10 bar and with stoichiometric O_2/CH_4 ratio. Small traces of homogenous combustion were always found, likely enhanced by the conditions of the experiments (reactor with large empty volume, occurrence of O_2 breakthrough, high preheating temperature of the inlet gas). In the presence of large amounts of H_2O and CO_2, the authors observed that pressure increase had a minor impact on the selectivity to syngas and the conversion of CH_4, possibly in line with the fact that the catalyst always operated within the mass transfer limited oxidation zone, being the conversion of O_2 incomplete. Spatially resolved measurements of temperature and composition within high density catalytic foams provided further insight in the effect of pressure in CH_4 CPO [4,7]. It is worthy to note that additional technical complexity has to be overcome when performing axially resolved measurements under pressurized conditions, due to the need of maintaining the reactor gas-tight while moving the probe. Bitsch-Larsen et al. [7] first performed CH_4 CPO experiments up to 11 bar over Pt- and Rh-coated 80 ppi alumina foams. When using Rh, tests at constant mass flow rate revealed almost no change both in temperature and concentration profiles, even though the residence time grew an order of magnitude passing from 1 to 11 bar. The surface hot spot (~1000 °C), the length of the oxidation zone (~3 mm) and the consumption profiles of the reactants maintained almost unaltered: variations were observed exclusively in the final part of the catalyst, once the reaction had approached the thermodynamic equilibrium. The results were interpreted as the clear indication that mass transport limitations govern both CH_4 and O_2 consumption under the conditions explored, as the authors demonstrated by evaluating the (weak) dependence of the transport processes on pressure and temperature. Providing further insight in the results of Ref. [7], more recently Horn and coworkers [4] were able to obtain spatially resolved profiles between 1 and 15 bar working on Pt-coated 80 ppi foams. Differently from Rh, which is so active in CH_4 CPO that mass transfer limitations become irreducible, kinetic effects were observed with Pt, which were associated to blockage of the catalyst surface by carbon formation and graphitization [14].

In the literature, the effect of pressure in the CPO of light hydrocarbons has been explored to a much lesser extent compared to CH_4 and, to the best of our knowledge, never by application of the spatially resolved sampling technique. In the case of C_3–C_6 hydrocarbons, several works report the presence of small fractions of cracking intermediates and olefins among the CPO products, already at atmospheric pressure [15–19]. It is then expected that gas phase chemistry plays a growing role at higher pressures, given the promotion of the kinetics. Coherently with these findings, during C_3H_8 CPO experiments conducted over honeycomb supported Rh catalysts, our group has reported the formation of C^{2+} intermediates in the first millimeters of the channel, as a consequence of the activation of homogenous chemistry [20,21]. Following these results, in the present work we analyze the autothermal CPO of C_3H_8 and CH_4, carried out between 1 and 4 bar (the safety operation limit of our lab) within an adiabatic reactor. Spatially resolved temperature and composition profiles are presented and analyzed with a numerical model of the reactor, which includes detailed schemes for gas phase and surface kinetics. We also report simulations up to 15 bar, which reveal that a significant growing share of C_3H_8 conversion (up to 45%) occurs in the gas phase via activation of oxidative dehydrogenation. The essential role of the catalyst in converting the olefinic intermediates by reforming is emphasized and confirmed by dedicated experiments.

2. Experimental and numerical tools

2.1. Catalytic materials

The CPO tests were performed over a 2 wt% Rh/α-Al_2O_3 catalyst supported onto a 400 cpsi cordierite honeycomb. The honeycomb was 26 mm long and 24 mm in diameter, with 75% open frontal area and 1.1 mm channel size. The catalyst was prepared by dry impregnation of the α-Al_2O_3 support (10 m^2/g surface area by BET measurement) with a commercial $Rh(NO_3)_3$ aqueous solution. Following a standard procedure, the catalyst was deposited over the honeycomb support by dip-coating and blowing-off of the slurry obtained from the catalyst powders. Adhesion of the deposited layer was achieved by subsequent drying at 280 °C in an oven for 15 min. The catalyst was deposited over the entire length of the monolith. The catalyst load (~800 mg) was estimated by weight difference before and after coating the monolith. The washcoat thickness (18 μm) was then calculated assuming a density of the catalyst layer of 1.38 g/cm^3. After the CPO experiments, the catalytic honeycomb was weighted. No loss of washcoat was found, confirming the good adhesion of the layer to the cordierite support. The metal dispersion was measured by CO and H_2 pulse chemisorption over powder samples, aged under representative conditions, and resulted equal to 20% according to both techniques.

2.2. Lab-scale reactor and operating conditions

Autothermal CH_4 and C_3H_8 CPO experiments were performed in the pressure range 1 to 4 bar, at constant 10 N l/min molar flow rate. In the case of CH_4 CPO experiments, CH_4/air mixtures with an O_2/C ratio of 0.57 were used (CH_4 = 27.4% v/v, O_2 = 15.7%, N_2 to balance). In the case of C_3H_8 CPO, the experiments were performed between 0.59 and 0.61 O_2/C ratio (C_3H_8 = 8.6%). The reaction was lit-off according to the following procedure: the catalyst was first heated by flowing a N_2 stream, kept at 500 °C by electric cartridges; when the catalyst temperature reached 350 °C, the N_2 stream was switched off and the reactants were fed separately to the catalyst from uninsulated lines at room temperature; once the ignition completed, the pressure was increased to the desired level. The experiments were performed 2 h after the light-off, to let the whole system (the catalyst and the insulated reactor) fully achieve the steady state. The gases were fed at room temperature for safety reasons: however, at steady state their temperature reached 40 °C at the entrance of the insulated adiabatic zone, due to conduction of the stainless-steel reactor and of the feed lines. The feed streams mixed in a FeCrAlloy foam (100 ppi, 2.2 cm long) placed upstream

of the catalyst. In the case of CH_4 the inlet composition was outside of the flammability limits at all pressures [22]. This was not the case with C_3H_8 at 3 and 4 bar: nonetheless, no trace of gas phase conversion was detected before the catalytic monolith, as proved by the axial profiles of concentration. This was likely due to the absence of an ignition source or to the flame-arresting properties of the mixing foam, given by the small diameter of the pores (~250 μm).

The reactor consisted of a stainless-steel tube, externally insulated by wrapping a thick pad of quartz wool. To prevent C formation, a quartz liner was used for hosting the catalytic monolith in the reactor. Within this liner, the catalytic monolith was placed in between two inert blank monoliths, kept at a distance of ~1 cm, which acted as heat shields. This choice increased the radiant heat dissipation at the edges of the catalytic monolith, thus preserving it from excessive heating, especially in the inlet portion [23]. The set-up of the reactor was modified to carry out spatially resolved measurements up to 4 bar. The sealing system was improved by addition of a guard filled with high vacuum grease (Dow Corning), which allowed to move the capillary and to avoid gas leakage. Specifically, the guard was composed of two parts, a 1/4 in. tube (8 cm long) connected to a 1/16 in. tube (5 cm long, 1 or 0.76 mm I.D. depending on the outer diameter of the capillary probe). In the longer part of the guard, the sealing was guaranteed by the large contact surface between the capillary and the grease. In the shorter part, the sealing was guaranteed by the formation of a film of grease between the outer wall of the capillary and the internal wall of the tube. The pressure of the reactor was measured at the inlet and was regulated with a control valve at the outlet. The reactor was also equipped with a pressure release valve located upstream of the catalyst to prevent overpressure. For the measurement of the spatially resolved concentration profile of the gas species, a deactivated fused silica capillary (O.D. = 350 μm, I.D. = 200 μm) was inserted into the central channel of the honeycomb and externally connected to a loop purposely designed for tests under pressure. The sampled flow (2 N cm^3/min) was carefully controlled by connecting the capillary to a regulation valve. After this valve, the sampled flow was admitted to an empty volume connected to a micro-GC (Agilent 3000). At each axial position, three composition measurements were repeated: C, H and O balances typically closed within ±5% error. For the spatially resolved measurements of temperature, the reactor was equipped with a K-type thermocouple (250 μm O.D.) and a narrow-band infrared pyrometer (Impac Infrared, IGA 5-LO) connected to an optical fiber (300 μm core diameter, 330 μm O.D.). A larger capillary (O.D. = 500 μm) sealed at one end was used to move the optical fiber and the thermocouple. The thermocouple measurements were taken as representative of the temperature of the gas phase, whereas the measurements of the pyrometer were representative of the temperature of the catalyst surface [24].

To estimate how close to the adiabatic limit the reaction was operated, a thermal efficiency parameter was calculated as the ratio between the experimental and the theoretical adiabatic temperature rise across the catalytic honeycomb. In the calculations, the inlet temperature was taken equal to 40 °C, as discussed. The theoretical temperature rise was estimated as the temperature increase predicted for an adiabatic reactor with the same performances of the real one, assuming the composition of the gas at the very outlet of the channel (26 mm). Also the experimental temperature rise was evaluated based on the temperature measured at the same axial position. In this way, the thermal efficiency parameter was more representative of the central channels of the monolith, where the sampling was performed. In the case of CH_4 CPO, the thermal efficiency was very close to unity. In the case of C_3H_8 CPO, given that the higher temperatures can damage the catalyst, a more heat-dissipative configuration was purposely adopted by removing the heat shields. This in turn enhanced the radiant dissipation at the edges of the monolith and caused the thermal efficiency to decrease to ~92% [23].

2.3. Mathematical model of the reactor and kinetic scheme

The experiments were analyzed with a 1D, adiabatic, heterogeneous, fixed-bed, single channel model of the reactor. The model consists of mass, enthalpy and momentum balances for the gas phase and for the solid phase. The model also includes axial convection and diffusion terms, solid phase conduction and gas–solid transport terms, estimated with correlations for laminar flow in square channels. Heat conduction in the solid was taken into account with an effective axial thermal conductivity coefficient, corrected by addition of the radiation contribution. The complete set of the equations is reported in Ref. [25]. The model includes kinetic schemes for the solid phase and for the gas phase. Gas phase reactions of C_1 to C_3 species were described according to the scheme proposed by Ranzi et al. [26]. This scheme consists of 1485 reactions and 82 species. It is able to account for the formation of species up to C_6 and of polyaromatics up to naphthalene: nonetheless, under the conditions investigated in the work, C_4 and larger species were found only in negligible amounts. The surface chemistry of C_3H_8 CPO was described according to the kinetic scheme recently reported by Pagani et al. [27], which upgrades a previous version reported in Ref. [28]. This scheme was derived on the basis of a dedicated experimental campaign, performed within an annular micro-reactor under quasi-isothermal kinetically-informative operating conditions, using 2-wt% Rh/α-Al_2O_3 catalysts analogous to the present one. The scheme extends a thermodynamically consistent microkinetic model for the description of CH_4 conversion over Rh catalysts [29] by adding two lumped steps for the activation of C_3H_8 under oxidative conditions and steam reforming conditions. These steps are the oxygen-assisted decomposition of C_3H_8 (Eq. (1)) and the decomposition of C_3H_8 in the absence of chemisorbed oxygen (Eq. (2)):

$$C_3H_8 + 3^* + 2O^* \rightarrow 3CH_2^* + 2OH^* \quad (1)$$

$$C_3H_8 + 5^* \rightarrow 3CH_2^* + 2H^* \quad (2)$$

For the oxygen-assisted decomposition step, the rate was assumed as first order dependent on the partial pressure of C_3H_8 and second order dependent on the fraction of chemisorbed O atoms:

$$r_{Ox} = k_{0,Ox} \times \exp\left(-\frac{E_{ATT,Ox}}{R} \times \left(\frac{1}{T} - \frac{1}{T_0}\right)\right) \times P_{C_3H_8} \times \theta_{O*}^2 \quad (3)$$

In the equation, the activation energy is 90 kJ/mol and $k_{0,Ox}$ is 4×10^{-6} mol/cm^2/atm/s (T_0 = 773 K). Similarly, the rate of the C_3H_8 decomposition step was assumed as first order dependent on the partial pressure of C_3H_8 and second order dependent on the fraction of free Rh sites:

$$r_{SR} = k_{0,SR} \times \exp\left(-\frac{E_{ATT,SR}}{R} \times \left(\frac{1}{T} - \frac{1}{T_0}\right)\right) \times P_{C_3H_8} \times \theta_{Rh}^2 \quad (4)$$

In this case, the activation energy amounts to 50 kJ/mol and $k_{0,SR}$ to 5.5×10^{-6} mol/cm^2/atm/s. Considering the results of Refs. [20,21], kinetic steps for the decomposition of some C_2 and C_3 intermediates (namely, C_2H_6, C_2H_4 and C_3H_6) were also required. In analogy with C_3H_8, the following lumped steps were added to the scheme:

$$C_2H_6 + 2^* \rightarrow 2CH_3^* \quad (5)$$

$$C_3H_6 + 3^* \rightarrow 3CH_2^* \quad (6)$$

$$C_2H_4 + 2^* \rightarrow 2CH_2^* \quad (7)$$

Table 1
Autothermal CH_4 CPO at increasing pressure. Comparison between experimental, calculated and thermodynamic results. The equilibrium was calculated at constant enthalpy and pressure.

P [bar]		χ CH_4 [%]	σ H_2 [%]	σ CO [%]	T_{OUT} [°C]
	Exp	88.5	90.3	86.6	686
1	Model	88.1	91.9	86.9	686
	Equil	*88.1*	*91.9*	*86.9*	*686*
	Exp	86.9	94.6	89.2	716
2	Model	85.9	90.4	86.5	716
	Equil	*85.8*	*90.5*	*86.4*	*718*
	Exp	85.7	92.6	88.6	738
3	Model	84.6	89.5	86.3	735
	Equil	*84.4*	*89.5*	*86.1*	*738*
	Exp	84.2	92.2	88.5	756
4	Model	83.6	88.8	86.1	749
	Equil	*83.3*	*88.7*	*85.8*	*751*

The rate dependences of these steps were assumed to be identical to that of C_3H_8 in the absence of chemisorbed oxygen (Eq. (4)) and the same kinetic parameters were used. Overall, the resulting scheme is able to predict the total oxidation and the steam reforming of C_3H_8 and CH_4, the oxidation of CO and H_2, the WGS and the RWGS reaction, as well as the methanation of CO and the steam reforming of C_2H_6, C_2H_4 and C_3H_6. Finally, it is worthy to note that all the simulations reported in this work were obtained on a fully predictive basis by introducing only the geometrical and the physical characteristics of the monolith, the measured Rh dispersion and the catalyst load.

3. Results and discussion

3.1. Effect of pressure in CH_4 CPO

The effect of pressure was first investigated in the case of CH_4 CPO between 1 and 4 bar under autothermal conditions. Fig. 1a and b show the axial profiles of temperature at the four pressures. In Fig. 1c–f, only the concentration profiles measured at 1 bar (●) and 4 bar (■) are reported, except for O_2 (for which data are reported at all the pressures). To better evaluate the integral performance, Table 1 provides a comparison among the experimental, the calculated and the thermodynamic values of temperature, CH_4 conversion and syngas selectivity at the outlet of the channel (~26 mm). The adiabatic equilibrium calculations are referred to an inlet temperature of 40 °C, due to a moderate effect of overheating of the inlet gas stream by the insulated stainless steel feed-lines (Section 2.2). Coherently with the adiabaticity of the reactor, reasonable agreement is found between the thermodynamic predictions and the experimental values at the outlet of the channel.

At all pressure values, the axial profiles are fully in line with previous spatially resolved CPO experiments, and with the results obtained by Bitsch-Larsen et al. [7]. O_2 and CH_4 are consumed in the first part of the catalyst, with production of synthesis gas and combustion products, followed by further consumption of CH_4 by steam reforming, as evidenced by the maximum in the concentration profile of H_2O. As a consequence of the balance between the exothermic oxidative chemistry and the endothermic reforming chemistry, a hot spot develops on the catalyst surface. The temperature of the gas phase, measured by the thermocouple, follows a similar evolution, with initial increase up to a maximum and subsequent decrease to the adiabatic limit. At the very first sight, the experimental profiles reveal that the catalyst is extremely active: within less than 10 mm from the inlet section, the reaction reaches the limit of adiabatic equilibrium and both temperature and concentration profiles are flat up to the end of the channel. Upon increasing the pressure, the hot spots of both the gas and the solid phases keep almost constant (Fig. 1a and b): the observed variations (±5 °C) are in fact within the precision of the experimental measurement. Correspondingly, also the consumption of O_2 and CH_4 and the length of the oxidation zone (~5 mm) maintain completely unchanged. Variations are observed only downstream of the hotspot: at increasing pressure, the temperatures increase from 680 to 757 °C, while the consumption of CH_4 and the production of syngas decrease. The result is explained on the basis of the expected thermodynamic trends: the adiabatic equilibrium involves a decrease of CH_4 conversion, a decrease of syngas selectivity and an increase of temperature. Overall, as previously noted in Ref. [7], the CH_4 CPO experiments show that pressure has a very limited effect on the kinetics, thus the variations observed being exclusively due to thermodynamics.

The model predictions are reported as solid lines in Fig. 1. The overall agreement is satisfactory with respect to both the axial profiles and the outlet values of temperature and concentration (Table 1), with modest underestimation of the temperatures after the hot spot. In this respect, it is worthy to recall that the simulations are entirely predictive and that all the important trends are retained and correctly followed, despite of the influence of the probe on the profile measured in the channel [30], including the insensibility of temperature and concentration profiles on pressure at the reactor inlet. An analysis of the model results allows to explain the phenomenon. In all the experiments, the consumption of O_2 was governed by external mass transport, as indicated by the calculated O_2 concentration profile at the catalyst wall (O_2^{wall}, Fig. 2a), which drops to zero immediately after the entrance of the channel. The occurrence of a mass transfer limited regime explains why neither the O_2 consumption profile nor the length of the oxidation zone change upon increasing the pressure. This point can be simply proved by assuming a Plug Flow behavior for the honeycomb channel and by considering that, under external mass transfer limited regime, the global consumption rate equals the mass transfer rate.

$$\frac{\dot{m}_{tot}}{A} \times \frac{d\omega_{O_2}^{Gas}}{dz} = -k_{m,O_2} \times a_v \times \rho_{Gas} \times \left(\omega_{O_2}^{Gas} - \omega_{O_2}^{Wall}\right) \quad (8)$$

In Eq. (8), A is the cross section of the channel, $\dot{m}_{tot}$ is the total mass flow of the gas, a_v the surface to volume ratio, ρ_{Gas} the density of the gas, k_{m,O_2} the mass transfer coefficient of O_2, and ω the mass fractions in the bulk of the gas phase and at the wall of the catalyst. Considering that $\omega_{O_2}^{Wall} = 0$ (Fig. 2a), a simple relationship between the consumption length and the mass fraction of O_2 is obtained:

$$\frac{d\omega_{O_2}^{Gas}}{\omega_{O_2}^{Gas}} = -\frac{A \times a_v \times k_{m,O_2} \times \rho_{Gas}}{\dot{m}_{tot}} \times dz \quad (9)$$

The independence of the oxidation length from pressure stems directly from the product between k_{m,O_2} and ρ_{Gas}. ρ_{Gas} has in fact a positive first order dependence on P ($\rho_{Gas} \propto P$ under the ideal gas assumption), while the mass transport coefficient k_{m,O_2} is inversely proportional on P ($k_{m,O_2} \propto P^{-1}$), as shown in Eq. (10) due to the dependence of gas diffusivity on P according to Fuller's correlation.

$$k_{m,i} = \frac{D_i^{mol} \times Sh}{d_{Channel}} \propto \frac{T^{3/2}}{P} \quad (10)$$

A similar situation emerges when the consumption of CH_4 is considered (Fig. 2b): the wall concentration is initially lower than the concentration in the gas bulk and progressively decreases up to reaching of the adiabatic equilibrium. In this zone (~5 mm), a very limited variation is predicted by the model at increasing pressure. Only downstream of this zone, the thermodynamic constraints cause the curves to separate. This result confirms that the

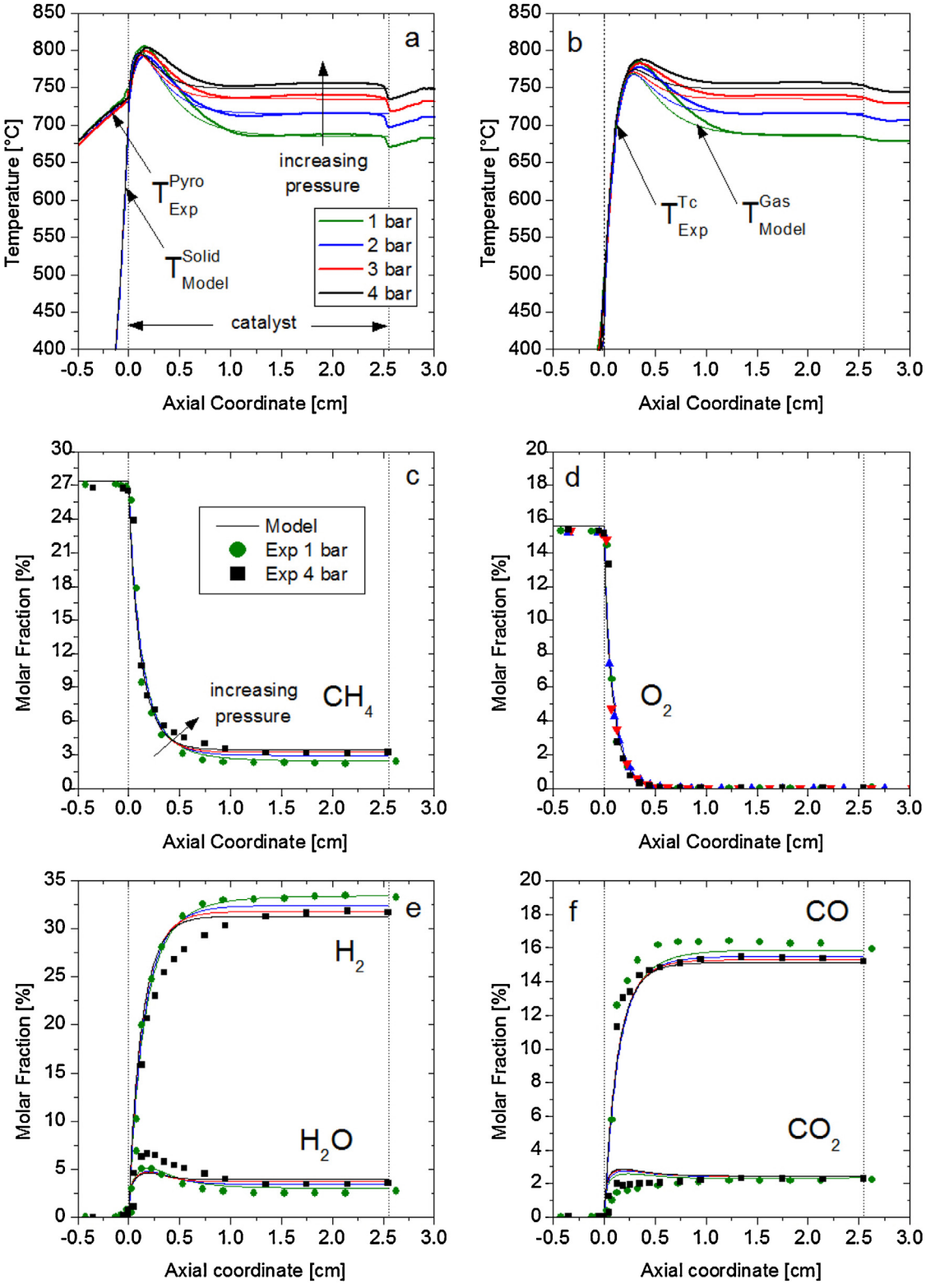

Fig. 1. Spatially resolved temperature and composition profiles for a CH_4 CPO experiment at increasing pressure from 1 (●) to 4 bar (■). Operating conditions: CH_4 = 27.4%, O_2/C = 0.57, T_{IN} = 40 °C, flow rate = 10 N l/min. Experimental measurements: symbol and thick lines in temperature profiles. Thin lines: model predictions.

external mass transport limitations prevail also in the case of CH_4, and therefore the same considerations made for O_2 hold for CH_4 consumption. Elsewhere, with Rh/α-Al_2O_3 catalysts supported over 400 cpsi honeycombs analogous to the present one [21], we showed that CH_4 consumption occurs in a mixed chemical-diffusive regime. Compared to the previous monoliths, the monolith used here have a higher catalyst load (~800 mg vs. ~620 mg), which in turn corresponds to larger active Rh area and larger chemical consumption rates. Consequently, given that the external transport rates are exclusively dictated by the honeycomb geometry and by the velocity profile, diffusion limitations are expected to have a greater impact, almost completely covering the

Table 2
Autothermal C_3H_8 CPO at increasing pressure. Comparison between experimental, calculated and thermodynamic results. The equilibrium was calculated at constant enthalpy and pressure. The experimental values are taken at 20 mm in Fig. 3.

P [bar]	O_2/C		χ C_3H_8 [%]	σ H_2 [%]	σ CO [%]	T_{OUT} [°C]
		Exp	100.0	92.7	93.7	793
2	0.59	Model	100.0	90.0	89.9	794
		Equil	*100.0*	*90.1*	*90.1*	*795*
		Exp	100.0	92.5	93.6	827
3	0.60	Model	100.0	88.9	89.5	826
		Equil	*100.0*	*89.1*	*89.8*	*826*
		Exp	100.0	88.9	90.8	851
4	0.61	Model	100.0	88.0	89.2	852
		Equil	*100.0*	*88.3*	*89.6*	*852*

residual kinetic effects. Finally, the mass-transfer control of O_2 and CH_4 consumption also explains why the hot spots of both the gas and the surface keep constant at increasing pressure (Fig. 1a). The consumption rates of O_2 and CH_4 are indeed the main contributors in the enthalpy balance, which determines the severity of the hot spot.

3.2. *Pressure effect in C_3H_8 CPO*

The results of spatially resolved experiments of C_3H_8 CPO carried out from 2 (▲) to 4 bar (■) are presented in Figs. 3 and 4. Table 2 provides a comparison among the experimental, the calculated and the thermodynamic values of temperature, C_3H_8 conversion and syngas selectivity at the outlet of the monolith. Model simulations are also reported as solid lines in Figs. 3 and 5. In Fig. 4, the lines only represent a link between the measured values.

As observed with CH_4, also in the case of C_3H_8 CPO the outlet temperatures increase going from 2 to 4 bar (Table 2). The measured axial profiles show that higher temperature levels are reached with C_3H_8 along the whole catalyst length if compared to CH_4 (e.g. at 4 bar, the maximum temperature of the surface is 951 °C in Fig. 3a vs. 802 °C in Fig. 1a). These higher temperatures enhance the heat dissipation by radiation at the edges of the monolith, as evidenced by the drop in the profiles after 20 mm. For this reason, the experimental values reported in Table 2 are taken at 20 mm along the axis of the channel. Coherently, the model simulations are in good agreement with the experimental curves in the central part of the channel, but overestimate the hot spot and the final part of the curves, given that the calculations were performed assuming the channel as adiabatic.

With respect to the axial evolution of the reactants and of the main products, a satisfactory agreement is found between model simulations and experiments. In the case of the intermediate hydrocarbon species (Fig. 4), the simulations qualitatively describe all the observed features, as shown in Fig. 5. Some quantitative lacks are present, which are likely due to the one-dimensional description of the monolith channel and to the interference of the sampling probe on the measured profile. Nonetheless, the agreement is reasonable and the simulations can be confidently used to better explain the data.

In analogy with CH_4 CPO, also in C_3H_8 CPO the consumption of O_2 is fully governed by external mass transport (Fig. 3d), as shown by the calculated zero concentration of O_2 at the catalyst wall (insert). Consequently, the O_2 consumption profile keeps constant at increasing pressure. Furthermore, given that the gas molar flow rate is the same in both C_3H_8 and CH_4 CPO experiments, the length of the oxidation zone maintains at ~5 mm, matching that of Fig. 1d. In contrast, pressure has a clear effect on the consumption of C_3H_8, which increases passing from 2 to 4 bar (between 0.25 and 1 cm, Fig. 3c). Together with CO_2, H_2O and syngas, formation of methane and C^{2+} products also occurs in this first part of the channel, where C_3H_8 is consumed (Fig. 4). As reported in previous works [20,21], these C_2^+ intermediates are formed in the gas phase by homogenous cracking chemistry and consumed on the catalyst surface by heterogeneous reforming chemistry. Coherently with this picture, the model simulations show that a peak is present in the profiles of methane and of the C^{2+} intermediates (Fig. 5). At increasing pressure, the maximum of these peaks is predicted to increase and to shift toward the inlet of the channel, due to the reduction of the residence time of the gas flow and to the promotion of the homogenous kinetics (which scales as P^2). For the C^{2+} species, at all the pressures investigated, the peak results from the balance between a positive global formation rate due to cracking and a negative global consumption rate by reforming (Fig. 6a, C_2H_4). The interaction between homogenous and heterogeneous

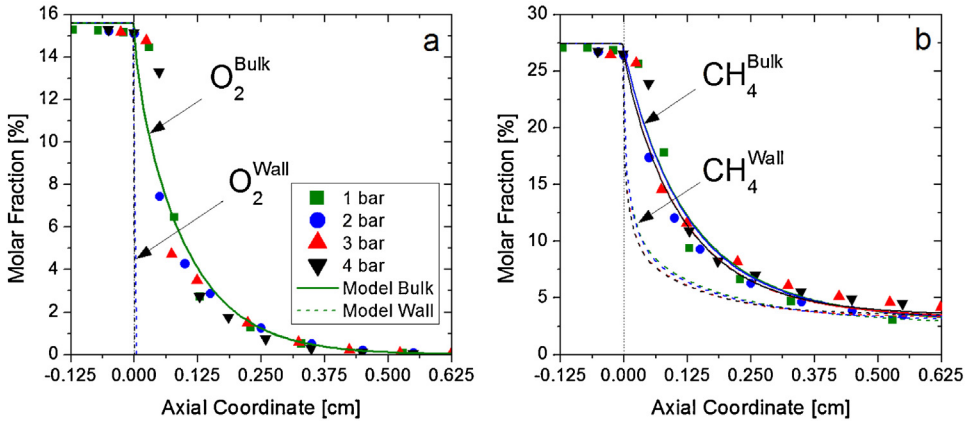

Fig. 2. Axial profile of O_2 (panel a) and CH_4 consumption (panel b). Operating conditions: CH_4 = 27.4%, O_2/C = 0.57, T_{IN} = 40 °C, flow rate = 10 Nl/min. Experimental measurements: symbol. Lines: model predictions.

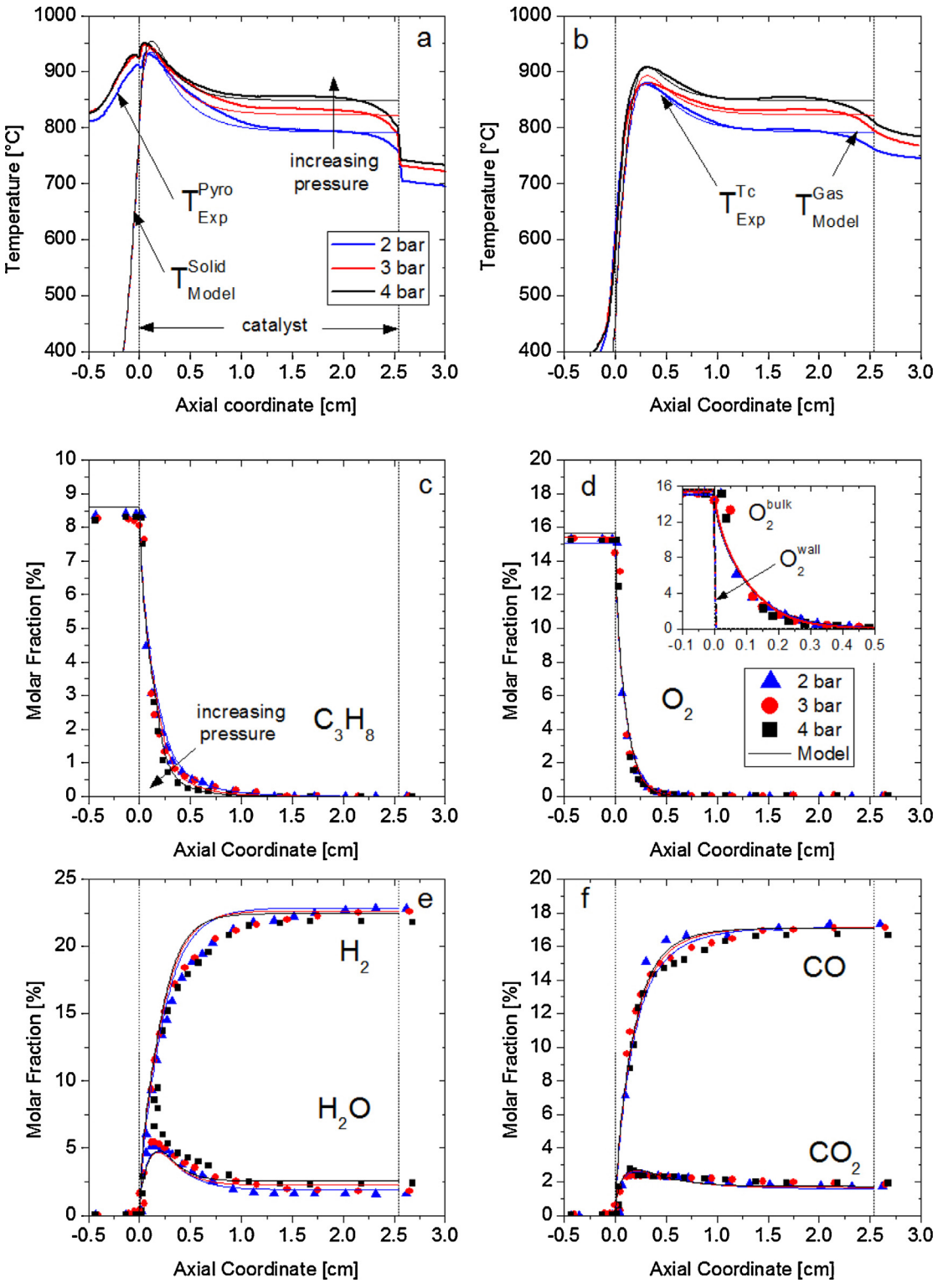

Fig. 3. Spatially resolved temperature and composition profiles for an autothermal C_3H_8 CPO experiment at increasing pressure. Operating conditions: C_3H_8 = 8.6%, O_2/C = 0.59–0.61, flow rate = 10 N l/min, P = 2 (▲), 3 (●) and 4 bar (■), T_{IN} = 40 °C. Experimental measurements: symbol and thick lines in temperature profiles. Thin lines: model predictions.

chemistry is more elaborate in the case of CH_4 (Fig. 6b): CH_4 is still formed by cracking and consumed by reforming, but additional production by methanation occurs in the final part of the monolith, which is responsible for the presence of CH_4 among the reaction products. Along with this, it is worthy to note that an increase of CH_4 production should be expected going from 2 to 4 bar, since the methanation equilibrium is promoted by pressure: however, in the present experiments, this promotion is not observed due to the variation of the O_2/C ratio in the feed (Table 2), as also confirmed by the model results (Fig. 5a).

The experimental and model results suggest that the promoting effect of pressure on the consumption of C_3H_8 is exclusively

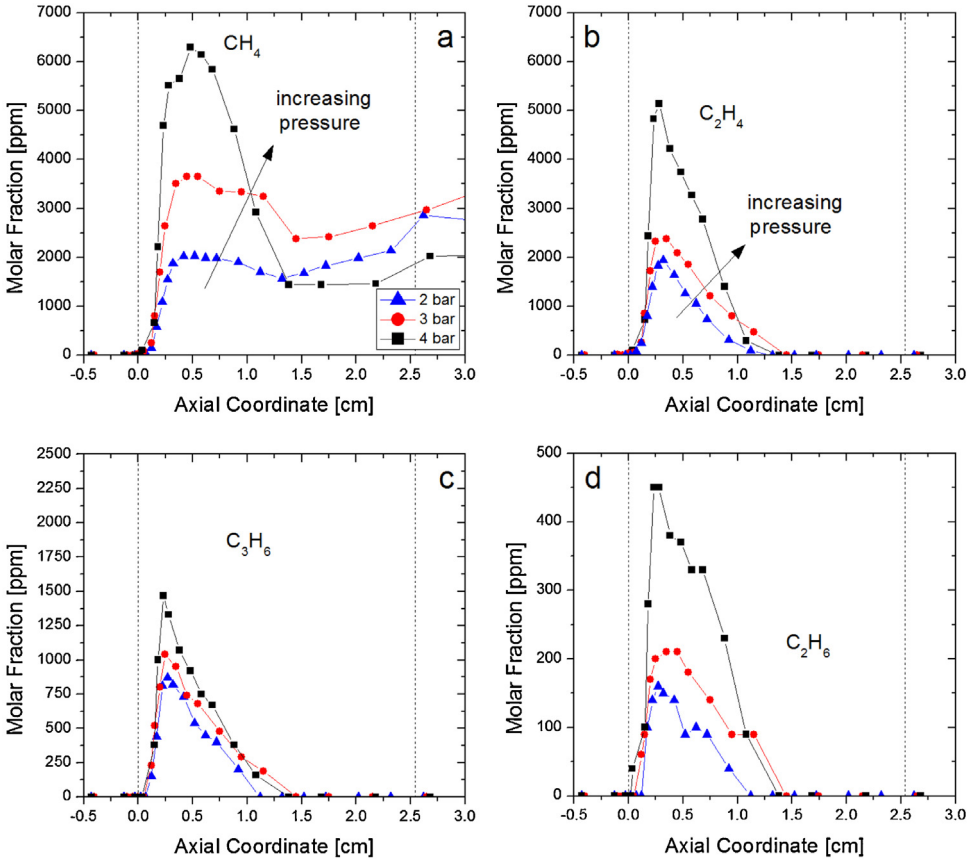

Fig. 4. Spatially resolved composition profiles of methane and C^{2+} products at increasing pressure from 2 to 4 bar. Conditions as in Fig. 3. Panels: CH_4 (a); C_2H_4 (b); C_2H_6 (c); C_3H_6 (d).

associated to the kinetics of the gas phase chemistry. Fig. 7 helps to illustrate this point: in this figure, the conversion of C_3H_8 to CO and CO_2 (i.e. the conversion mainly due to surface chemistry, panel a) and the conversion of C_3H_8 to CH_4 and C^{2+} species (i.e. the gas phase conversion, panel b) are reported for the first 15 mm of the channel for 2 to 4 bar. The calculations are based on the carbon material balance, which is fulfilled with an error of ±5% at each axial point. Within the experimental precision, it is clearly seen that the conversion to CO and CO_2 keeps constant between 2 and 4 bar, while the gas phase conversion increases up to a share of ~10% at 4 bar. Hence, pressure has no effect on the heterogeneous chemistry, rather it exclusively promotes the contribution of the homogenous cracking chemistry, which acts as an additional side-route for C_3H_8 conversion. The independence of the heterogeneous conversion from pressure confirms that external mass transfer limitation governs the consumption of C_3H_8 at the catalyst surface. This result is not unexpected: in fact, compared to CH_4, whose conversion is governed by mass transfer (Section 3.1), C_3H_8 has higher kinetic rates for total oxidation and steam reforming, but a lower diffusion coefficient. Likewise, also the conversion of the C^{2+} intermediates to syngas is limited by external mass transfer, due to the fact that their diffusion coefficient is lower than that of CH_4 and their reforming rates are comparable to those of C_3H_8. Thus, it can be concluded that, under the conditions analyzed, the external diffusive limitations govern all the surface reactions, making their kinetics insensitive to pressure: the pressure increase kinetically favors only the homogenous reactions, resulting in the increase of the amount of the intermediate hydrocarbon species produced.

3.3. *Role of the gas phase intermediates*

The intermediate C^{2+} species generated in the gas phase are carbon precursors that can lead to formation of coke on the catalyst surface. The characteristic peak observed during C_3H_8 CPO is associated with the coupling between homogenous cracking reactions and heterogeneous reforming reactions, which act as a chemical quench and are therefore essential for preventing coking phenomena. In a previous work [20], the key role of the heterogeneous reforming chemistry was proved numerically by showing that the measured temperature and concentration profiles cannot be reconciled without taking into account endothermic reforming steps for the C^{2+} species. In order to experimentally verify these conclusions, in the present work a C_3H_8 CPO test was carried out at 4 bar and 15 N l/min over a 8 mm long 400 cpsi honeycomb, washcoated with the 2-wt% Rh/α-Al_2O_3 catalyst. On the one hand, pressure accelerates exclusively the kinetics of the homogenous reactions (Section 3.2). On the other hand, the short catalyst length and the high flow rate reduce the residence time enough to avoid the complete reforming of the C^{2+} species. The resulting residence time is however long enough to guarantee significant conversion of O_2 and to produce high local temperatures. To allow for the gas phase chemistry to proceed, a large empty volume was also provided after the catalytic "slice".

The results of this experiment are summarized in Fig. 8, which reports the concentration profiles of CH_4 and C^{2+} species along the axis of the catalyst and in the empty reactor volume downstream. A neat breakthrough of CH_4 and C^{2+} olefins is achieved after the initial

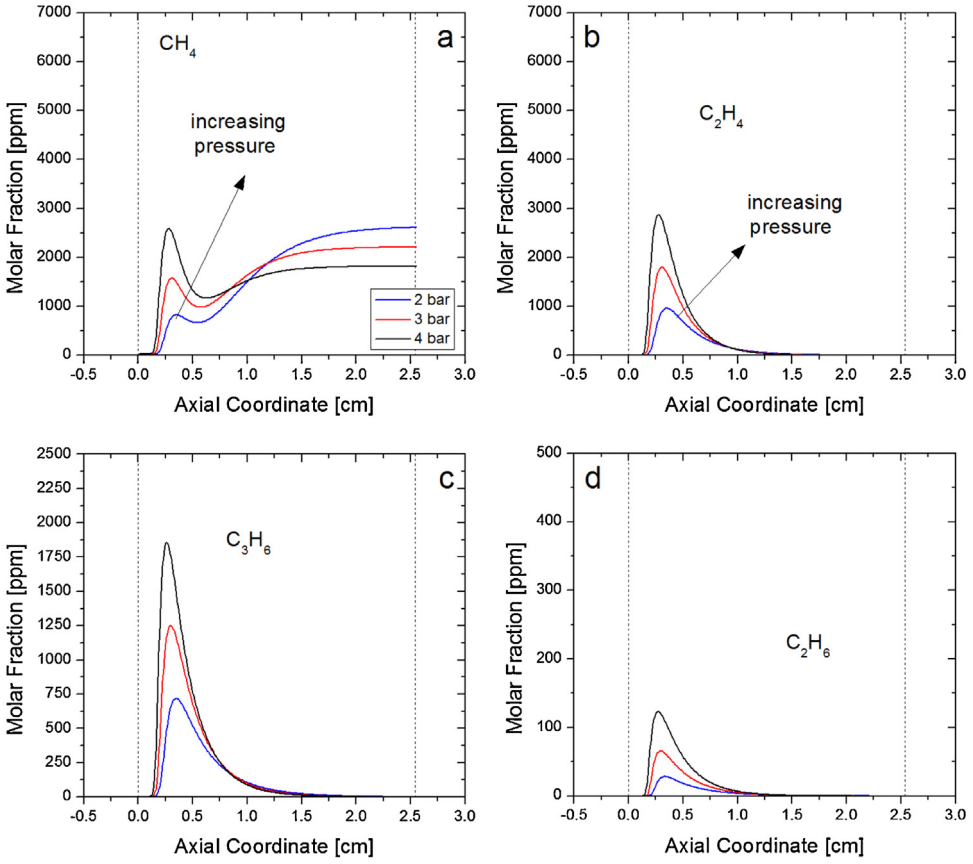

Fig. 5. Calculated profiles for a C_3H_8 CPO experiment at increasing pressure. Conditions as in Fig. 3. P = 2 (blue line), 3 (red line) and 4 bar (black line). Panels: CH_4 (a); C_2H_4 (b); C_2H_6 (c); C_3H_6 (d). (For interpretation of the references to colour in this figure legend, the reader is referred to the web version of this article.)

peak (likely a consequence of the incomplete reforming process). Downstream of the catalyst, the concentration of these species grows significantly due to the gas phase chemistry. The equimolar production of CH_4 and C_2H_4 suggests that propane mainly cracks according to Eq. (11), with a minor contribution from reactions (12) and (13).

$$C_3H_8 \rightarrow CH_4 + C_2H_4 \quad (11)$$

$$C_3H_8 \rightarrow C_3H_6 + H_2 \quad (12)$$

$$C_2H_4 + H_2 \rightarrow C_2H_6 \quad (13)$$

The experiments confirm that the heterogeneous reforming of gas phase intermediates plays a key role in C_3H_8 CPO: the catalyst surface acts as a chemical quench, preventing the build-up of short hydrocarbons and their condensation to polycyclic aromatic species and possibly coke.

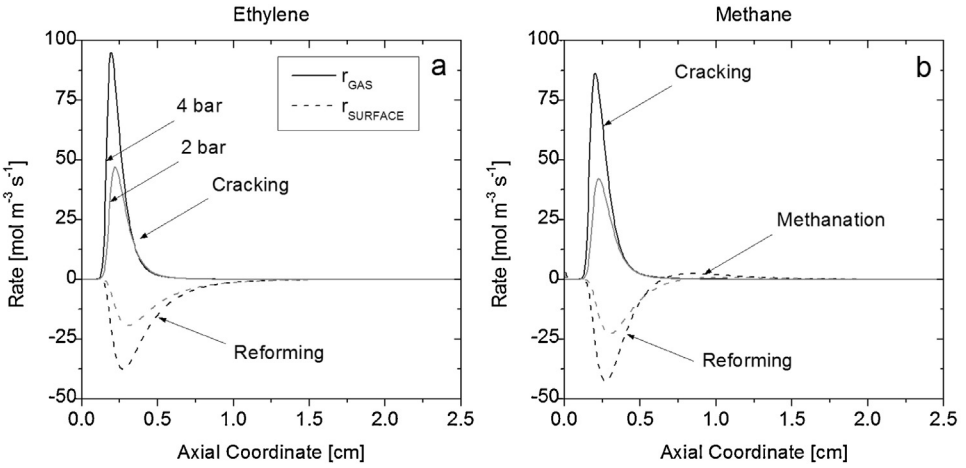

Fig. 6. Calculated global formation and consumption rates for C_2H_4 (a) and CH_4 (b) along the axis of the catalyst. Conditions: C_3H_8 = 8.6%, O_2/C = 0.59, flow rate = 10 N l/min, P = 4 bar.

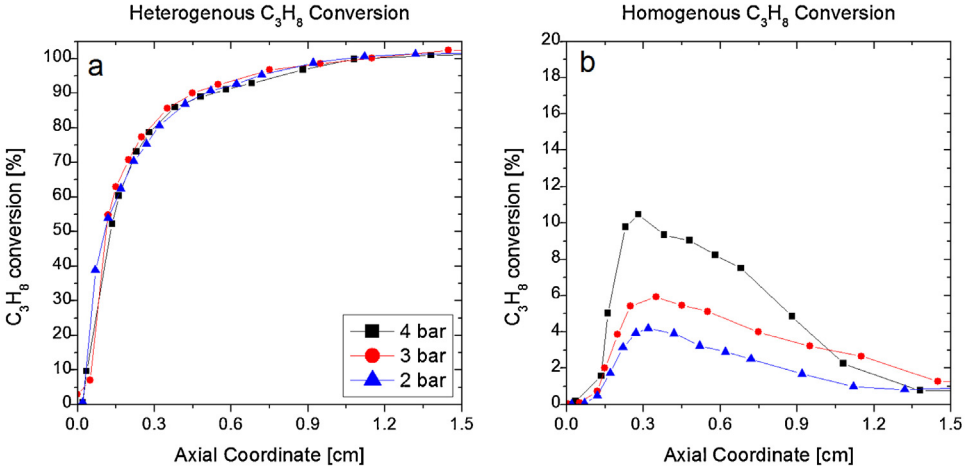

Fig. 7. Calculated conversion of C_3H_8. Heterogeneous conversion to CO and CO_2 (panel a); homogenous conversion to methane and C^{2+} products (panel b).

3.4. C_3H_8 CPO simulations up to 15 bar

One main conclusion arises from the analysis of the spatially resolved C_3H_8 CPO data: due to the strong impact of diffusive limitations, the heterogeneous conversion routes are kinetically insensitive to pressure. Pressure retains a kinetic effect only on the gas phase routes. It is then interesting to simulate the results of C_3H_8 CPO experiments under more severe conditions, for instance up to 15 bar, in order to verify to what extent the homogenous chemistry proceeds and whether the reactor is still able to reform the olefin intermediates. Simulations are reported in Fig. 9 for the case of C_3H_8 CPO experiments between 4 and 15 bar, with 8.6% C_3H_8, O_2/C ratio of 0.59 and a flow rate of 10 N l/min. In the figure, the curves at 4 bar are kept as a reference for the comparison. Qualitatively, the reactor response is maintained: the higher is the pressure, the higher become the outlet temperatures and the selectivity to CH_4, with lower production of syngas. However, as pressure increases, the contribution of the gas phase chemistry grows at the expenses of the surface chemistry: the rate of C_3H_8 consumption increases (Fig. 9c) with larger peak production of CH_4 (panel f), C_2H_4 (panel f, insert) and of all the other hydrocarbon intermediates. According to the simulations, traces of acetylene and C^{4+} species are also formed, but no breakthrough of these intermediates occurs at the end of the honeycomb. This means that the contact time is long enough to attain the maximum syngas selectivity. Noteworthy, at increasing pressure, the gas phase chemistry starts to involve also O_2 (panel c, insert), which reacts predominantly with C_3H_8 and C_2H_6 via oxidative dehydrogenation (Eqs. (14) and (15)) and with H_2, giving extra production of H_2O (panel d), propylene and ethylene.

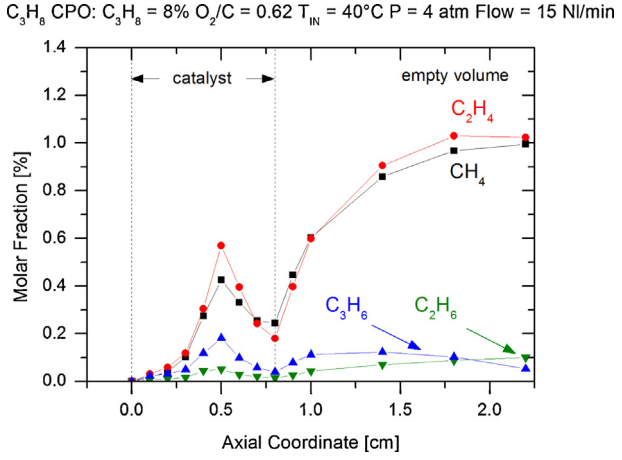

Fig. 8. Spatially resolved temperature and composition profiles for a C_3H_8 CPO experiment performed over a 8 mm catalyst slice. Operating conditions: C_3H_8 = 8%, O_2/C = 0. 62, flow rate = 15 N l/min, P = 4 bar, T_{IN} = 40 °C. Profiles of temperature (a) and molar fractions of reactants (b), heterogeneous products (c) and gas phase products (d).

$$C_3H_8 + 0.5O_2 \rightarrow C_3H_6 + H_2O \quad (14)$$

$$C_2H_6 + 0.5O_2 \rightarrow C_2H_4 + H_2O \quad (15)$$

Gas phase production of CO and CO_2 also occurs (panel e) due to partial oxidation and combustion contributions that overlap with the oxidative dehydrogenation steps.

As a consequence of the fact that the oxidative chemistry is partially taking place directly in the bulk of the gas, the hot spot temperature of the gas phase increases with increasing pressure (from 925 °C at 4 bar to 1040 °C at 15 bar, Fig. 9b). Additionally, as pressure grows, O_2 is consumed in a shorter volume (Fig. 9a, insert): the density of the heat release increases and the gas temperature profiles become steeper. On the other hand, progressively lower amounts of O_2 react on the catalyst via highly exothermic total oxidation pathways, causing the surface hot spot to decrease (from 981 °C at 4 bar to 925 °C at 15 bar, Fig. 9a). As a matter of fact, the results of Fig. 9 reveal that upon increasing the pressure, the reaction progressively skips out of the surface and transfers to the gas phase. To better illustrate this point, it is worthy to analyze the global consumption rate of C_3H_8 and O_2 due to gas phase reactions and to surface reactions. Between 4 and 15 bar, the rate of C_3H_8 consumption due to gas phase reactions (continuous lines, Fig. 10a) is predicted to grow up to one order of magnitude, and the associated fraction of C_3H_8 conversion passes from 15% to 45% (Fig. 10b). At 4 bar, the rate of surface consumption (dashed lines) is always higher than the rate of the gas phase reactions. At 15 bar, between 0 and 1 mm, as long as the gas phase chemistry has not ignited, the surface chemistry prevails and its rate maintains equal to that at 4 bar due to the external diffusive control (the dashed lines at 4 and 15 bar overlap, Fig. 10a). Once the radical chemistry ignites in the gas phase, the rate of the surface chemistry drops. This drop is due to the fact that C_3H_8 is depleted by consumption in the gas phase and its flow to the catalyst wall decreases as a consequence of the decrease of the gas-bulk concentration. An analogous picture can be drawn for O_2: at 4 bar the contribution of gas phase chemistry is almost negligible (Fig. 10a, insert), while at 15 bar the concentration effect causes the heterogeneous conversion rate to drop once the homogenous reactions activate.

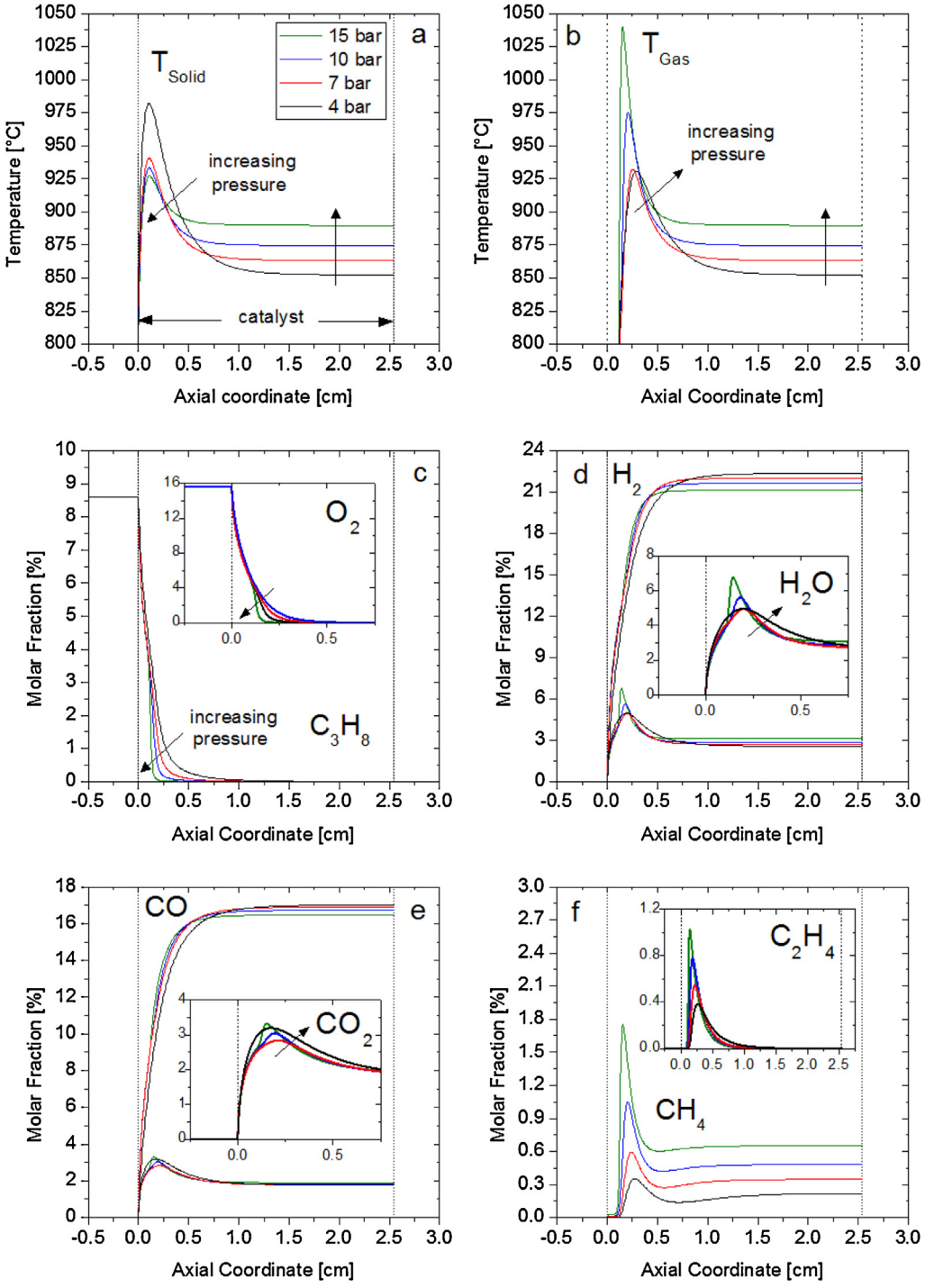

Fig. 9. Calculated temperature and composition profiles for an autothermal C_3H_8 CPO experiment at increasing pressure from 4 to 15 bar. C_3H_8 = 8.6%, O_2/C = 0.59, flow rate = 10 N l/min. Profiles of temperature ((a) and (b)), molar fractions of reactants (c) and products ((d)–(f)).

The corresponding fraction of O_2 conversion amounts to 27%. The results of panels a and b also tell that the stoichiometry of the consumption of O_2 and C_3H_8 in the gas phase passes from a C_3H_8/O_2 ratio of ~0.5 at 7 bar to a ratio of ~1 at 15 bar, in line with the growing importance of oxidative dehydrogenation and partial oxidation reactions. At 4 bar, instead, the conversion of C_3H_8 in the gas phase is almost entirely due to cracking, with a limited contribution by O_2 (2.6% of the total conversion). This change in the consumption stoichiometry also means that the gas phase chemistry passes from weakly exothermic (4 bar) to highly exothermic (15 bar). This point is well evidenced by estimating the total power density due to the gas phase reactions and to the surface reactions. Panel c and d of Fig. 10 report these power densities, calculated as $\sum_j^{NR} r_j \times \Delta H_j^R$ along the axis of the catalyst. In the gas phase, it can be seen that the balance is always positive between 4 and 15 bar, that is, the oxidative contributions prevail over the endothermic ones: upon increasing the pressure, the amount of heat released increases, which is the reason why progressively higher hot spot temperatures are found in the gas phase (Fig. 9b). For comparison, the figure reports also the curve calculated at 1 bar, which

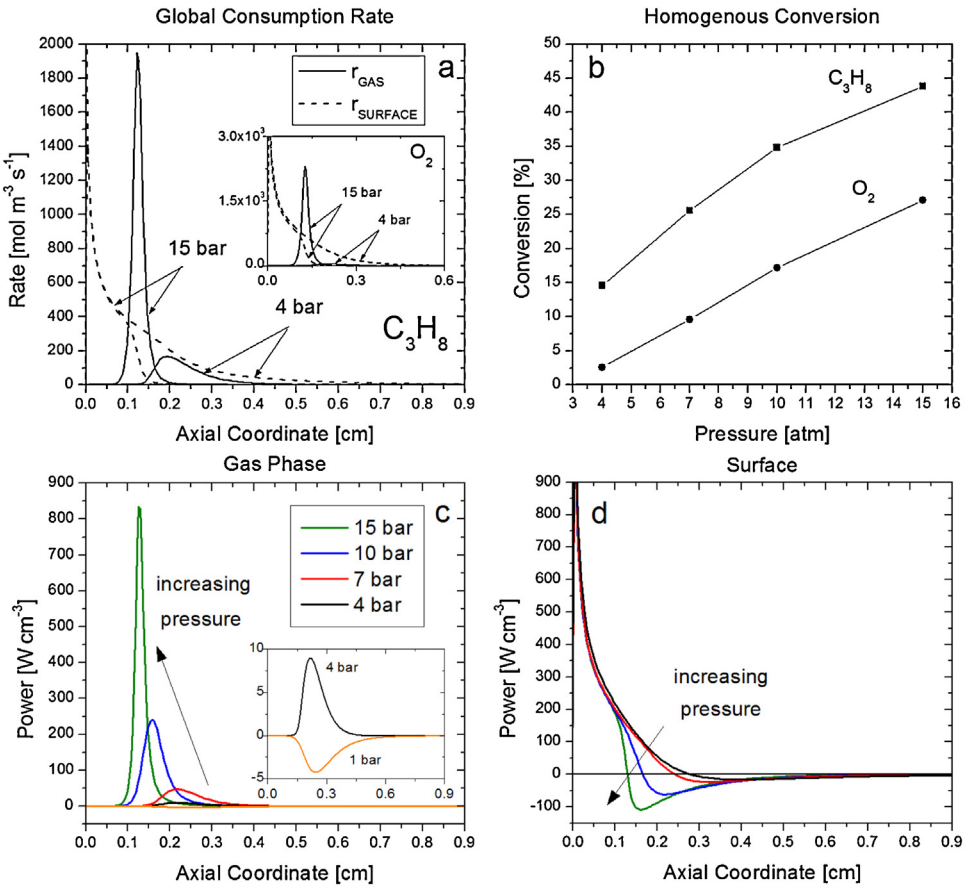

Fig. 10. Global consumption rates of C_3H_8 and O_2 (a); homogenous conversion of O_2 and C_3H_8 (b); power output due to gas phase chemistry (c) and surface chemistry (d). Conditions as in Fig. 9.

represents the limiting case wherein only the endothermic cracking reactions occur since no O_2 is converted in the gas. On the catalyst surface, the exo-endothermic sequence typical of the CPO reaction is maintained: however, as pressure increases, a smaller amount of heat is produced by the total oxidation reactions and lower hot spot temperatures are reached. As a matter of fact, a 27% reduction of the heterogeneous O_2 conversion allows for a moderation of the surface hot spot of 50 °C (Fig. 9a). Notably, the heating of the gas phase due to pressure also causes the ignition point of the homogenous chemistry to move toward the inlet of the catalyst, from 0.12 cm at 4 bar to 0.05 cm at 15 bar (Fig. 10a). This effect is in line with a thermal flashback mechanism: at sufficiently high pressures (at 20 bar under the conditions adopted in the calculations), the process reaches the point where the reaction is ignited before the entrance of the catalyst.

Overall, one of the most interesting results emerging from the simulations is that the ignition of gas phase chemistry allows for a significant moderation of the catalyst hot spot. The effect is double-sided: on the one hand, the gas phase chemistry forces the fuel to crack into smaller species that diffuse more easily across the boundary layer, increasing the rate of heat removal via reforming. On the other hand, a significant fraction of O_2 is consumed homogenously, so that the heterogeneous chemistry releases a lower amount of heat. Hence, the moderation of the surface temperatures stems from a synergy between the gas phase chemistry, which acts as a promoter of the gas mixture diffusivity by fragmentation of the fuel, and the heterogeneous chemistry, which selectively produces synthesis gas and avoids the formation of coke by reforming the olefins. As a matter of fact, provided that the catalyst is active enough, the capability of completely reforming the intermediate hydrocarbon species is associated to the geometric characteristics of the catalyst (i.e. channel length and height), since the consumption of these species is also governed by external mass transfer (Section 3.2). This picture can be possibly extended to the activation of heavier fuels, more bulky than C_3H_8, which have higher enthalpy of reaction and lower diffusivity coefficients than C_3H_8. As well, the activation of gas phase chemistry changes the heat distribution within the CPO reformer, changing the strategies for its thermal optimization compared to low pressure. At low pressure, the moderation of the hot spot is achieved by tuning exclusively the heterogeneous chemistry, either promoting the endothermic reforming by increase of the catalytic activity (catalyst load or active area), or moderating the oxidative heat release by optimization of the mass transfer properties of the support (aspect ratio, channel size). Under pressurized conditions, the gas phase conversion represents an additional parameter in the reactor design that needs to be tuned properly. For instance, increasing the channel size slows down the heat released by heterogeneous oxidation and favors the onset of the homogenous chemistry, thus positively affecting the surface temperatures: however, the gas phase chemistry is non-selective to synthesis gas and sufficiently long channels are needed to reform the intermediate olefins produced. In contrast, a small channel size limits the extent of homogenous chemistry but leads to a higher surface hot spot, which can be detrimental for the catalyst. As a matter of fact, the presence of homogenous chemistry changes the paradigm of the exo-endothermic balance typical of CPO at low pressure: novel design criteria must then be envisaged for the reactor to perform the CPO of C_3H_8 and other light hydrocarbons under pressurized conditions.

4. Conclusions

The experimental and numerical analysis of methane and propane CPO reformers at pressures below 4 bar show that pressure has mainly a thermodynamic effect on the integral performance of the reactor and leads to an increase of the outlet temperature. In the inlet portion of the catalyst, where the process and thus the evolution of concentration and temperature profiles are controlled by kinetics, pressure has a negligible effect due to the prevailing role of mass transfer limitations on the consumption of O_2 and of the fuel. This in turn results from the fact that the gas–solid diffusion rate in honeycombs is totally independent of pressure under laminar flow regime (and constant mass flow rate), causing the rate of the heterogeneous consumption to be insensitive to pressure. Consequently, no change is observed in the hot spot temperature, a highly critical parameter for the durable operation of a CPO reformer.

Instead, the role of homogenous reactions is seen to grow with increasing pressure. Which especially affects the performance of a C_3H_8–CPO reformer. While, in fact, in the case of CH_4, no evidence of homogenous chemistry was observed below 4 bar, gas phase reactions contributed to C_3H_8 conversion through the intermediate formation of C^{2+} olefins and methane in the same pressure range, with no appreciable impact on the thermal behavior.

Upon further increasing the pressure, numerical simulations reveal that homogenous oxidative dehydrogenation chemistry activates and that a significant fraction of the reactants is converted in the gas phase (up to 45% and 28% of C_3H_8 and O_2 conversion, respectively, at 15 bar). This has a negligible impact on the final productivity of syngas, since the hydrocarbons formed by the gas phase reactions further react on the catalyst surface contributing, together with the incoming fuel, to the steam reforming process. Instead, most importantly, the partial conversion of O_2 in the bulk phase produces a decrease of the O_2 flow to the catalyst surface, with a beneficial effect on the thermal load and a net decrease of the catalyst hot spot temperature.

In conclusion, data and simulations suggest that the control of mass transfer limitations on the rate of heterogeneous reactions and the onset of homogeneous reactions "protect" the catalyst surface from a worsening of the thermal stress at increasing pressure. This appears an extremely interesting and "comforting" result in view of the intensification of CPO short contact time reformers.

References

[1] L. Basini, K. Aasberg-Petersen, A. Guarinoni, M. Ostberg, Catalysis Today 64 (2001) 9–20.
[2] C. Willich, C. Westner, M. Henke, F. Leucht, J. Kallo, K.A. Friedrich, Journal of the Electrochemical Society 159 (2012) F711–F716.
[3] B.J. Dreyer, P.J. Dauenhauer, R. Horn, L.D. Schmidt, Industrial & Engineering Chemistry Research 49 (2010) 1611–1624.
[4] O. Korup, R. Schlogl, R. Horn, Catalysis Today 181 (2012) 177–183.
[5] O. Deutschmann, L.D. Schmidt, AIChE Journal 44 (1998) 2465–2477.
[6] C.T. Goralski, L.D. Schmidt, Chemical Engineering Science 54 (1999) 5791–5807.
[7] A. Bitsch-Larsen, R. Horn, L.D. Schmidt, Applied Catalysis A: General 348 (2008) 165–172.
[8] A.G. Dietz, L.D. Schmidt, Catalysis Letters 33 (1995) 15–29.
[9] M. Fichtner, J. Mayer, D. Wolf, A. Schubert, Industrial & Engineering Chemistry Research 40 (2001) 3475–3483.
[10] J.K. Hong, L.Z. Zhang, M. Thompson, W. Wei, K. Liu, Industrial & Engineering Chemistry Research 50 (2011) 4373–4380.
[11] M. Lyubovsky, S. Roychoudhury, R. LaPierre, Catalysis Letters 99 (2005) 113–117.
[12] C. Appel, J. Mantzaras, R. Schaeren, R. Bombach, A. Inauen, N. Tylli, M. Wolf, T. Griffin, D. Winkler, R. Carroni, Proceedings of the Combustion Institute 30 (2005) 2509–2517.
[13] A. Schneider, J. Mantzaras, R. Bombach, S. Schenker, N. Tylli, P. Jansohn, Proceedings of the Combustion Institute 31 (2007) 1973–1981.
[14] O. Korup, S. Mavlyankariev, M. Geske, C.F. Goldsmith, R. Horn, Chemical Engineering and Processing: Process Intensification 50 (2012) 998–1009.
[15] A.G. Dietz, A.F. Carlsson, L.D. Schmidt, Journal of Catalysis 176 (1998) 459–473.
[16] M. Hartmann, T. Kaltschmitt, O. Deutschmann, Catalysis Today 147 (2009) S204–S209.
[17] M. Huff, P.M. Torniainen, L.D. Schmidt, Abstracts of Papers of the American Chemical Society 206 (1993) 127–130.
[18] B.C. Michael, D.N. Nare, L.D. Schmidt, Chemical Engineering Science 65 (2010) 3893–3902.
[19] B. Silberova, H.J. Venvik, A. Holmen, Catalysis Today 99 (2005) 69–76.
[20] A. Donazzi, D. Livio, M. Maestri, A. Beretta, G. Groppi, E. Tronconi, P. Forzatti, Angewandte Chemie International Edition 50 (2011) 3943–3946.
[21] D. Livio, A. Donazzi, A. Beretta, G. Groppi, P. Forzatti, Industrial & Engineering Chemistry Research 51 (2012) 7573–7583.
[22] M.G. Zabetakis, Flammability Characteristics of Combustibles Gas and Vapors, U.S. Department of Interior—Bureau of Mines, Washington, 1965.
[23] D. Livio, A. Donazzi, A. Beretta, G. Groppi, P. Forzatti, Topics in Catalysis 54 (2011) 866–872.
[24] A. Donazzi, D. Livio, A. Beretta, G. Groppi, P. Forzatti, Applied Catalysis A: General 402 (2011) 41–49.
[25] A. Donazzi, M. Maestri, B.C. Michael, A. Beretta, P. Forzatti, G. Groppi, E. Tronconi, L.D. Schmidt, D.G. Vlachos, Journal of Catalysis 275 (2010) 270–279.
[26] E. Ranzi, A. Frassoldati, R. Grana, A. Cuoci, T. Faravelli, A.P. Kelley, C.K. Law, Progress in Energy and Combustion Science 38 (2012) 468–501.
[27] D. Pagani, A. Donazzi, M. Maestri, A. Beretta, G. Groppi, P. Forzatti, Industrial & Engineering Chemistry Research (2013), under review.
[28] D. Pagani, D. Livio, A. Donazzi, A. Beretta, G. Groppi, M. Maestri, E. Tronconi, Catalysis Today 197 (2012) 265–280.
[29] M. Maestri, D.G. Vlachos, A. Beretta, G. Groppi, E. Tronconi, AIChE Journal 55 (2009) 993–1008.
[30] M. Hettel, C. Diehm, B. Torkashvand, O. Deutschmann, Catalysis Today (2013), http://dx.doi.org/10.1016/j.cattod.2013.05.005, in press.